Title

Development of sub-100 femtosecond timing and synchronization system

Journal

Review of Scientific Instruments, 89(1)

ISSN

0034-6748

Authors

Lin, Zhenyang
Du, Yingchao
Yang, Jin
et al.

Publication Date

2018

DOI

10.1063/1.5001768

Peer reviewed

Review of Scientific Instruments

Development of sub-100 femtosecond timing and synchronization system

Cite as: Rev. Sci. Instrum. **89**, 014701 (2018); https://doi.org/10.1063/1.5001768
Submitted: 26 August 2017 . Accepted: 05 December 2017 . Published Online: 02 January 2018

Zhenyang Lin, Yingchao Du, Jin Yang, Yilun Xu, Lixin Yan, Wenhui Huang, Chuanxiang Tang, Gang Huang, Qiang Du, Lawrence Doolittle, Russell Wilcox, and John Byrd

AIP Publishing

Development of sub-100 femtosecond timing and synchronization system

Zhenyang Lin,[1] Yingchao Du,[1] Jin Yang,[1,2] Yilun Xu,[1,2] Lixin Yan,[1] Wenhui Huang,[1,a)] Chuanxiang Tang,[1] Gang Huang,[2,b)] Qiang Du,[2] Lawrence Doolittle,[2] Russell Wilcox,[2] and John Byrd[2]

[1]*Department of Engineering Physics, Tsinghua University, Beijing 100084, China*
[2]*Lawrence Berkeley National Laboratory, Berkeley, California 94720, USA*

(Received 26 August 2017; accepted 5 December 2017; published online 2 January 2018)

The precise timing and synchronization system is an essential part for the ultra-fast electron and X-ray sources based on the photocathode injector where strict synchronization among RF, laser, and beams are required. In this paper, we present an integrated sub-100 femtosecond timing and synchronization system developed and demonstrated recently in Tsinghua University based on the collaboration with Lawrence Berkeley National Lab. The timing and synchronization system includes the fiber-based CW carrier phase reference distribution system for delivering stabilized RF phase reference to multiple receiver clients, the Low Level RF (LLRF) control system to monitor and generate the phase and amplitude controllable pulse RF signal, and the laser-RF synchronization system for high precision synchronization between optical and RF signals. Each subsystem is characterized by its blocking structure and is also expansible. A novel asymmetric calibration sideband signal method was proposed for eliminating the non-linear distortion in the optical synchronization process. According to offline and online tests, the system can deliver a stable signal to each client and suppress the drift and jitter of the RF signal for the accelerator and the laser oscillator to less than 100 fs RMS (~0.1° in 2856 MHz frequency). Moreover, a demo system with a LLRF client and a laser-RF synchronization client is deployed and operated successfully at the Tsinghua Thomson scattering X-ray source. The beam-based jitter measurement experiments have been conducted to evaluate the overall performance of the system, and the jitter sources are discussed. *Published by AIP Publishing.* https://doi.org/10.1063/1.5001768

I. INTRODUCTION

High precision, long-term, and long-distance transfer synchronization among RF, laser, and beams plays an important role in the photocathode injector based applications such as MeV ultrafast electron diffractions,[1–4] x-ray free electron laser,[5–7] and Thomson scattering x-ray source.[8–11] The jitter of the RF-RF, RF-laser, or laser-beams should be seriously controlled to sub-100 femtosecond level to generate low jitter high-quality X-ray or electron pulses and to achieve high time resolution with pump-probe experiments in these facilities.

In general, the timing and synchronization system consists of the phase reference distribution system (PRDS) and other subsystems for related clients such as the laser oscillator (laser-RF synchronization) and the accelerator RF [low level RF (LLRF)]. Although waveguide or coaxial cable solution is simple, it is sensitive to the environment temperature leading to its difficulty in achieving sub-picosecond stability in long-term operation.[12,13] Over the last decade, the optical fiber based solutions including the balanced optical pulse laser cross-correlator method from MIT[14,15] and the continuous laser carrier based method from Lawrence Berkeley National Lab (LBNL)[16,17] have been quickly developed. The optical fiber based solution can achieve femtosecond to several hundred attoseconds level synchronization in kilometer scale facilities.[14–16,21–23] Based on the different phase reference distribution systems, the corresponding scheme of the clients can be selected. The digital LLRF system has been developed over a decade with wide application in most accelerator facilities. It is more flexible and convenient in algorithm implementation and timing control in comparison with analog signal processing.[17–20] In addition, there are also two main laser-RF synchronization schemes in modern accelerator systems depending on the type of the timing system (pulse or CW).[15–20]

To provide precise timing and synchronization for Tsinghua high-brightness beam research, the Tsinghua Accelerator Lab, cooperating with LBNL, has been investigating on the integrated timing and synchronization system for several years. The PRDS, LLRF system, and laser-RF synchronization system are integrated, and the whole femtosecond timing and synchronization system has been established, which was successfully demonstrated at the Tsinghua Thomson scattering X-ray (TTX) source.[24–27] The preliminary testing results show that the LLRF system with the PRDS can achieve typically 46 fs RMS phase jitter under the closed loop (in 24 h, 2856 MHz RF frequency) and the typical absolute integral phase jitter of the laser-RF synchronization system with the PRDS is 83.2 fs RMS (10 Hz–100 kHz).

In this paper, we will present the details of the system and the preliminary testing results at the TTX. Together with the basic theory of the three subsystems in Sec. III, Sec. II mainly presents the scheme of the Tsinghua femtosecond timing and synchronization system. Sections IV A and IV B

a)huangwh@mail.tsinghua.edu.cn
b)GHuang@lbl.gov

present the long-term experiment of the subsystems and its application at the TTX and discusses the phase jitter sources and the improvement methods of subsystems in detail. Besides, Sec. IV C introduces the beam-based jitter measurement experiment to make the whole performance assessment of the whole deployed timing and synchronization system.

II. THE SCHEME OF TSINGHUA TIMING AND SYNCHRONIZATION SYSTEM

The Tsinghua timing and synchronization system has an integrated hardware construction which includes a reference RF oscillator, a timing laser source module, a sync-head chassis, a receiver chassis, an event distribution module, and related connection cables and fibers, as shown in Fig. 1. The reference RF oscillator generates a low noise signal from a high-performance phase-locked 119 MHz oscillator by frequency multipliers including the 2856 MHz reference signal and 79.3 MHz signal for event distribution and laser phase locking and the 404.6 MHz signal for Field Programmable Gate Array (FPGA) clock. To meet the 100 fs level timing requirements for multi-clients, the timing laser source module provides the modulated reference laser signal and is mainly consisted of the fiber-based CW carrier source (Koheras ADJUSTIK E15), modulator, Rb-lock module (under deploying), erbium-doped fiber amplifier (EDFA), and sender parts. The linewidth of the CW laser is less than 0.1 kHz (Lorentzian), and the coherence length is several hundred kilometers. It is enough for the km level accelerator, and the linewidth influence is negligible. The stability of the laser wavelength is ~0.1 pm/°C, and the temperature is controlled by electrical temperature controllers (~0.1 °C), where $\frac{\Delta\lambda}{\lambda} = \frac{0.01\times10^{-12}}{1550\times10^{-9}} == 6.5\times10^{-9}$. For the scale of the TTX is less than 100 m, the estimated additional jitter from it is 2.2 fs ($dt = d\lambda/\lambda \times t = 6.5\times10^{-9} * 100/3\times10^{8} = 2.2$ fs), which can be ignored.[16] The rest of the signal processing parts are physically divided into the sync-head chassis and the receiver chassis for different working environment. The receiver chassis consists of the core RF phase detector and corrector based on the LLRF4.6 board and should be far away from the accelerator hall to avoid strong radiation.[24–26] The feedback signal is generated from the receiver chassis to the devices under control for closed loop phase locking. The sync-head chassis locates close to the signal pickup point to minimize uncontrolled cable delay and does the photoelectric signal demodulation and preliminary signal processing. Moreover, we configure the event distribution module from Micro-Research Finland (MRF) to distribute the 10 Hz timing events, which includes the master time base and Event Generator (EVG) and Event Receiver (EVR).

The standard modules and chassis of the THU timing and synchronization system characterizes by its integrated structure, and they are suitable for manufacture, debugging, and expansion. As illustrated in Fig. 1, the PRDS contains all three parts: timing laser source module, the sync-head chassis, and the receiver chassis. The LLRF system and the laser-RF synchronization system have the same hardware configuration which includes the sync-head chassis and the receiver chassis. Such a design is convenient for deployment and later maintenance in large scale facilities.

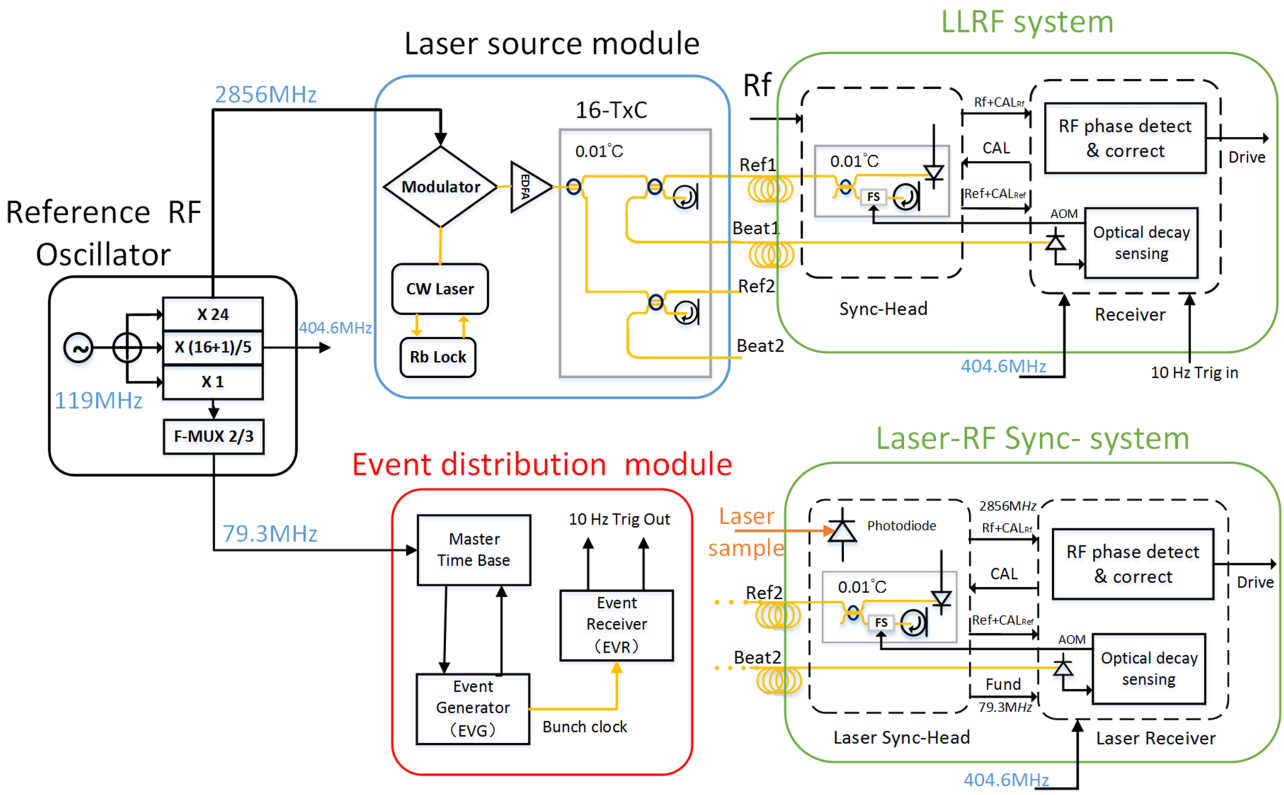

FIG. 1. The scheme of the timing and synchronization system in THU.

The system phase noise is still an important issue in timing and synchronization system evaluation. The noise is mostly from broadband electronic noise, flicker noise, thermal pickup, and acoustic pickup. Besides, feedback loops can suppress low frequency noise up to a point determined by the gain-BW of the system. The broadband electronic noise is a white noise that can be minimized by a choice of lower noise components. The LLRF system bandwidth is limited by the pulse repetition rate, and the laser control loop bandwidth is limited by the piezoelectric ceramic transducer (PZT) response time and the whole control loop delay. As a result, the phase noise from different subsystems and their combination will be a critical evaluation criterion of the timing and synchronization system.

III. THE SUBSYSTEMS OF THE TIMING AND SYNCHRONIZATION SYSTEM

In the timing and synchronization system, the LLRF system and laser-RF synchronization system are integrated together with the PRDS in the sync-head chassis and the receiver chassis, which adopts the similar hardware. Each subsystem is charged with specific responsibilities and coordinates mutually.

A. CW laser modulated phase reference distribution system

The phase reference distribution system (PRDS) aims at keeping the phase error of different remote-clients less than dozens of femtoseconds all the time. According to Fig. 1, the RF signal is loaded on a continuous laser by the intensity modulation. The modulated optical signal (Ref fiber) is sent to the far end of the fiber and the light intensity is detected by a photodiode, which is set in the sync-head chassis. The phase error of the RF signal distribution can be obtained precisely by measuring the optical phase delay based on the beat signal on the fiber using heterodyne interferometry.

The sync-head chassis is designed as an enclosed aluminum box thermally isolated from the environment. The internal temperature is controlled by the Peltier cooler with 0.01 °C temperature drift to suppress its influence on the fibers of interferometers out of the feedback loop. The beat signal of the interferometer carries this delay variation information, and it is also sent to the receiver side over another fiber. At the receiver side, the modulated RF signal is detected from the laser by a photodiode, and the phase of the detected RF $Ø_{det}$ is[16]

$$Ø_{det} = -2\omega_{op}t_{ref} - 2\omega_{FS}\left(t_{ref} + t_{beat}\right) + 2Ø_{FS}, \qquad (1)$$

where t_{ref} is the delay time of an optical wave propagating through the reference fiber, t_{beat} is the delay time of an optical wave propagating through fiber beat, ω_{op} is the optical frequency (2π * 200 THz), ω_{FS} is the frequency shifter RF frequency (2π * 55 MHz), and $Ø_{FS}$ is generated by the frequency shifter for control. With the application of a local phase control loop (LLRF or mode-locked laser controller), the propagation delay drift can be compensated so that all controlled client devices can be synchronized together.

The sync-head chassis and the receiver chassis are placed in different areas as mentioned before. They are connected with cables which should be the same length and go through the same path to ensure the constant phase difference between reference and RF signals. However, the phase difference is sensitive to the slight distinction of the two cables caused by the temperature and shakiness under S-band frequency. Therefore, a calibration signal (CAL) is applied to measure and compensate the phase difference drift caused by the connection cables variation between the sync-head chassis and the receiver chassis. If the length of any cable on the signal processing link changes, it is possible to simultaneously monitor the phase difference change between the reference and RF signals by the calibration signal in the reference cable (Cal_{ref}) and the calibration signal in the RF cable (Cal_{rf}). The signal error is accurately corrected in the signal process algorithm.[17,24–26]

B. Low level RF control system

Low level RF systems close the feedback loop around the high-power RF system and the cavity, stabilizing the accelerating field observed by the beam. The pulse-to-pulse feedback control mode is a common way to be chosen for the LLRF system, where the amplitude and phase information of the previous pulse signal is used to feed back the next pulse signal. In the case of short-pulse RF systems, such feedback cannot depress jitter but the long-term errors are categorized as drift.

According to Fig. 2, the Tsinghua LLRF system includes the sync-head chassis and the receiver chassis. The receiver chassis is placed outside of the accelerator hall with the solid-state amplifier, modulator, and klystrons. The coupling RF signal from the electron gun is sent into the sync-head chassis. Besides, this part of cable should be as short as possible since it is out of the control loop. The cavity RF signal was sent back to the LLRF receiver chassis through the coaxial cable along with the reference signal. Moreover, the LLRF system measures the RF signals from the accelerator electron gun, compares it with the phase reference received from the PRDS, calculates the phase error, and provides the driving RF signal to the high-power RF system (solid state amplifier and klystron). Then, the RF signal is fed into the electron gun and the accelerator tube to provide synchronized RF for the electron beam.

The system closed-loop phase error of the cables between the sync-head and the receiver is obtained from the coupling probe through the calibration signal (CAL), the calibration signal in the reference cable (Calref), and the calibration signal in the RF cable (Calrf). The CAL signal is generated from the receiver, which is a time-delay pulse signal in the time domain in comparison with the pickup RF signal from the accelerator. In the pulse signal chain, the mixed CAL signal with the RF pulse signal in the time domain can be easily separated by reasonable timing control to calculate the CAL signal phase φ_{cal_rf}. However, for the reference signal channel, the reference signal is superimposed with the CAL signal in the time domain. In the I/Q plane, the reference signal and the CAL signal vector are added. The phase value of the calibration signal in the reference signal φ_{cal_ref} can be obtained with the I/Q value of the CAL signal by recording the I/Q value of the mixed signal

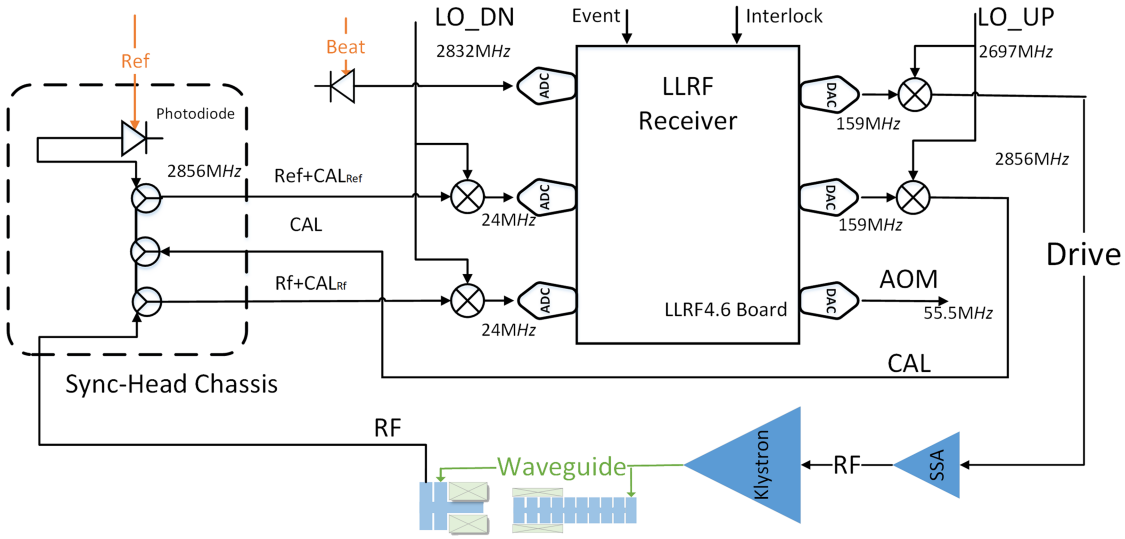

FIG. 2. The configuration of the LLRF system.

and the pure reference signal,

$$I_{cal\_ref} = \left(I_{ref+cal} - I_{ref}\right),$$
$$Q_{cal\_ref} = \left(Q_{ref+cal} - Q_{ref}\right). \tag{2}$$

Then, we can obtain the phase error after the compensation,

$$\nabla\varphi = \left(\varphi_{rf} - \varphi_{ref}\right) - \left(\varphi_{Cal\_rf} - \varphi_{Cal\_rf}\right). \tag{3}$$

The frequency of the accelerator RF signal is 2856.00 MHz. In terms of the signal down-convert, the LO signal frequency is 2832.20 MHz, and the RF signal frequency is down converted from 2856.00 MHz to 23.80 MHz and then sent to the LLRF4.6 board. The output signal frequency of the LLRF4.6 board is 158.67 MHz, and its frequency is up-converted from 158.67 MHz to 2856.00 MHz with 2697.33 MHz LO signal. Both the signal down-convert and up-convert processes are conducted in the discrete devices, respectively, before and after the signal DSP in the LLRF receiver chassis. The signal core processing module are integrated into the FPGA board including the timing control module, amplitude and phase detector module, feedback calculation module, and output module. The LLRF DSP scheme is shown in Fig. 3. The two ADC channels are used to measure the reference, RF signal (24 MHz), and their mixture with CAL signals separately. The signals go through the digital demodulator with the Look-up-Table-based frequency mixer, Cascade Integrator-Comb (CIC) filter, and Non-in-phase and quadrature (IQ)[28] sample to get the IQ values. The IQ packets are split to obtain the amplitude and phase information of REF, RF, and CAL with precise timing control, and the errors can be derived under the error compensation algorithm. Proportional-integer controller is applied to complete the feedback calculation and CORDIC-based Direct Digital Synthesis (DDS) for phase and amplitude calculation to get the driver signal DAC output (158.67 MHz). The receiver side of the PRDS shares the same hardware and firmware with the LLRF system, so the receiver chassis uses two LLRF4.6 boards as an integrated timing receiver and LLRF controller.[24–26]

C. Laser-RF synchronization system

Laser-to-RF conversion and synchronization are crucial for further implementation after the fiber-based PRDS distributing the optical timing reference. The Tsinghua accelerator lab has conducted on the harmonic phase noise measurement method where the research was proceeded by

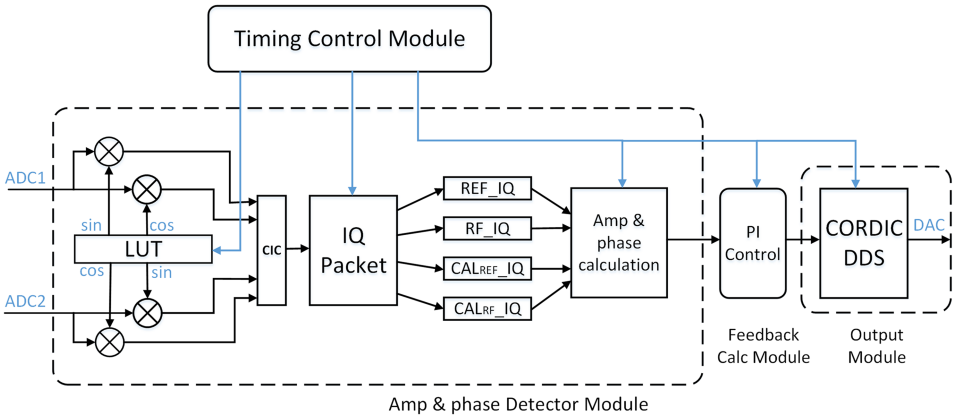

FIG. 3. The DSP scheme of the LLRF system.

applying phase mixing and filtering technology to measure the phase error.[27] However, the DC bias output of the phase detector leads to aliasing between signal amplitude and the phase noise, which affects the efficiency of the phase detector to discriminate the phase error and carries the amplitude modulation-phase modulation (AM-PM) phase distortion. In addition, a new digital phase detector with the heterodyne method is applied to eliminate such conversion errors and is flexible to configure different algorithms with the digital phase identification method.[24,25]

The typical laser-RF synchronization system in THU contains laser the sync-head chassis, the receiver chassis, and the feedback control module, as shown in Fig. 4. The laser oscillator output optical pulse signal goes through an optical splitter and feeds into the photodiode detection. The laser oscillator repetition rate is 79.33 MHz with 36 periods S-band harmonic (2856.00 MHz) in each fundamental period. The laser oscillator is locked to both S-band (2856.00 MHz) harmonic and the fundamental frequency (79.33 MHz) of the laser signal for high precision phase-locked of laser oscillators. If the laser pulse is just locked to a specific phase of one of the harmonic periods, there is no determination of which one it is. Therefore, a fundamental sub-harmonic frequency is required to help resolve this bucket ambiguity, which can be derived from a separate sub-harmonic distribution line (from the PRDS) to synchronize all receiver chassis. As for the jitter measurement principle, the jitter of a certain harmonic frequency laser (σ_E) consists of the amplitude noise (σ_E) and phase noise (σ_J) contributions. The selection of a high harmonic carrier frequency would be highly benefited from a low amplitude noise contribution. Consequently, in the following measurements, the 36th harmonic (2856.00 MHz) is also chosen to represent the phase jitter, so the contribution of amplitude noise can be ignored.[27]

The fundamental frequency and harmonic frequency of the laser signal are, respectively, filtered out in the laser-RF synchronization sync-head. Besides, the harmonic frequency (2856.00 MHz) signal is combined with the double sideband suppressed carrier calibration signal (Cal) coming from the receiver chassis as well as the phase reference signal.[17] The corresponding signal was sent to the receiver chassis to extract relative phase information with the application of the heterodyne method. The core signal processing board calculates the final phase deviation through the PI feedback algorithm to control the amount of feedback as the LLRF system. According to different laser oscillators, the output port has self-adaptive adjustment. The two typical control ports are the laser oscillator piezoelectric ceramic transducer (PZT) for the slow DAC to change the length of the laser oscillator optical resonant cavity and the stepper motor for coarse adjustment if the cavity length changes acutely.

1. The solution of the third-order intercept point (IP3) with CAL signal in laser-RF synchronization system

Compared with the LLRF system, the calibration signal in the laser-RF synchronization system is in different forms since the RF signal is continuously detected from the photodiode. The double sideband suppressed carrier CAL signal is applied to be added on the Ref and RF signals in the laser-RF synchronization system. There will be 3 spectrum lines after combining the RF and double sideband suppressed carrier Cal signals for the intermodulation among them by the nonlinear effects of components. Such a third-order intercept point will introduce significant distortion to the corrected signal.[17] As shown in Fig. 5(a), the red line is the reference fiber signal with external interference, about 217 ps peak-peak phase distortion caused by heating. The black line is the corrected reference signal phase with the CAL signals in the PRDS. Besides, the periodic fluctuation of the black line brings remarkable 2.37 ps peak-peak phase error, which is different from the expectation to be a linear curve. For the fluctuation keeps pace with the changing reference signal, the IP3 is the main origination which leads to the signal distortion.

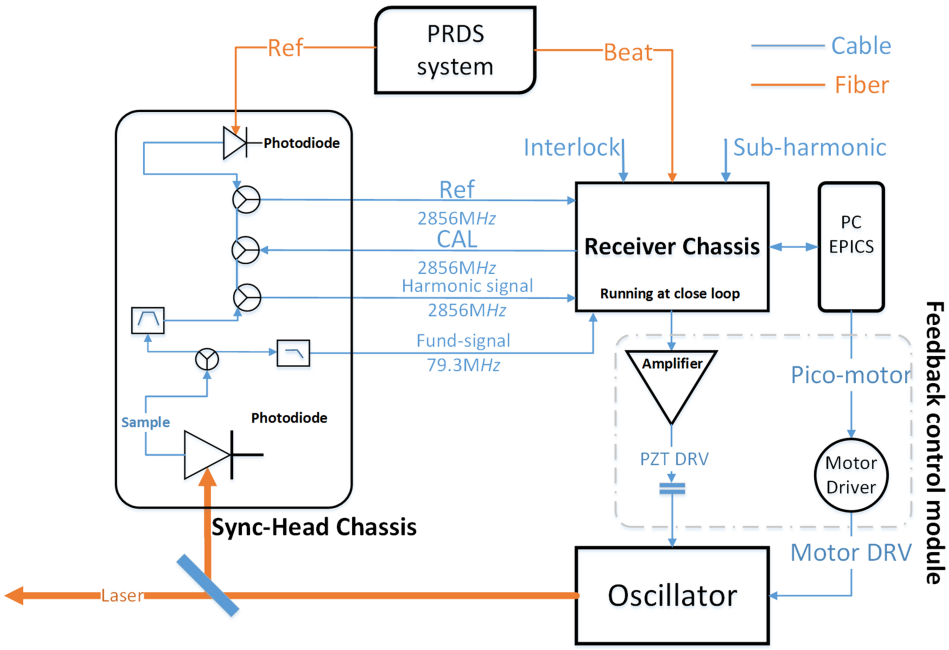

FIG. 4. The configuration of the laser-RF synchronization system.

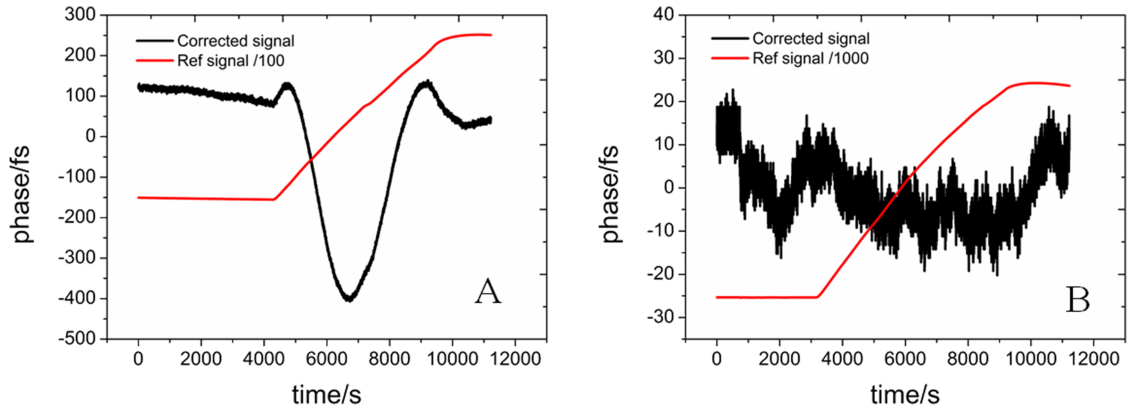

FIG. 5. The IP3 phenomenon and its suppression between laser sync-head and receiver in the laser-RF synchronization system. (a) The ref signal has about 217 ps peak-peak phase distortion caused by external interference, and the corrected ref signal notable distortion caused by IP3 has reached 2.37 ps peak-peak by heating. (b) The IP3 is repressed with the asymmetric sideband CAL signal method, and the phase distortion has been reduced to 36.82 fs RMS.

Therefore, to eliminate the non-linear distortion in the process, an asymmetric calibration sideband signal was proposed and applied. The double sideband of the Cal signal is adjusted to $f_0 - \Delta f_1$ and $f_0 + \Delta f_2$, where the Δf_1 is 1.19 MHz and Δf_2 is the 3.57 MHz. Besides, we change the coefficient of the phase error equation

$$\nabla\varphi = \left(\varphi_{rf} - \varphi_{ref}\right) - \left(\varphi_{Cal\_up,rf} - \varphi_{Cal\_dw,rf}\right)/2 - \left(\varphi_{Cal\_up,ref} - \varphi_{Cal\_dw,ref}\right)/2 \quad (4)$$

to

$$\nabla\varphi = \left(\varphi_{rf} - \varphi_{ref}\right) - \left(\varphi_{Cal\_up,rf}{}^{*}\mathrm{a} - \varphi_{Cal_{dw},rf} * b\right)/2 - \left(\varphi_{Cal\_up,ref}{}^{*}\mathrm{a} - \varphi_{Cal_{dw},ref} * b\right)/2, \quad (5)$$

where $a + b = 1$. For the symmetric system, the weight of Cal_up and Cal_dw is the same and $a = b = 0.5$ by linear interpolation. However, in the asymmetric system, the coefficient should be calculated based on practical tests and measurements.

According to Fig. 5(b), the asymmetric calibration sideband method works effectively to correct the phase distortion of the ref signal to 36.82 fs RMS (a = 0.65, the algorithm of dichotomy was applied to find the optimum value of a), indicating that the reference signal phase can be distributed precisely from the sender to laser LLRF receiver chassis with the interferometer.

IV. EXPERIMENTS OF THE TIMING AND SYNCHRONIZATION SYSTEM AT TTX

The primary timing and synchronization system was deployed for the two clients in the Tsinghua Thomson scattering X-ray (TTX) source,[24–26] which includes the LLRF system for accelerating RF stabilization and the laser-RF synchronization system for photocathode drive laser phase locking, which can be found in Fig. 6.

The laser-RF synchronization sync-head and receiver are closely put in the clean room with the laser oscillator, while the pickup laser sample from the oscillator are sent into the laser sync-head for feedback. The mode-locked laser oscillators are locked to the distributed reference signal. The laser amplifiers are not included in the control loop because the repetition rate (10 Hz) is too low. The LLRF sync-head is set near the electron gun signal pickup as closely as possible with a short cable, and the LLRF receiver is put in the klystron room. The RF driver signal from the receiver goes through the solid-state amplifier (SSA) and klystron to feed into the gun and tube via the waveguide.

Series performance tests have been carried out to evaluate the performance of the system including a mutual monitoring and detecting between two LLRF subsystems before commissioning and the tests of each subsystem after the deployment.

A. LLRF subsystems' mutual monitoring and detecting experiments

The RF signal generated by the LLRF subsystem signal is in a pulse form, which is not easy to be measured by a traditional signal source analyzer. As a result, a mutual monitoring and detecting between two LLRF subsystems method is proposed where an independent LLRF system is applied to measure the other one before the system commissioning at the TTX.

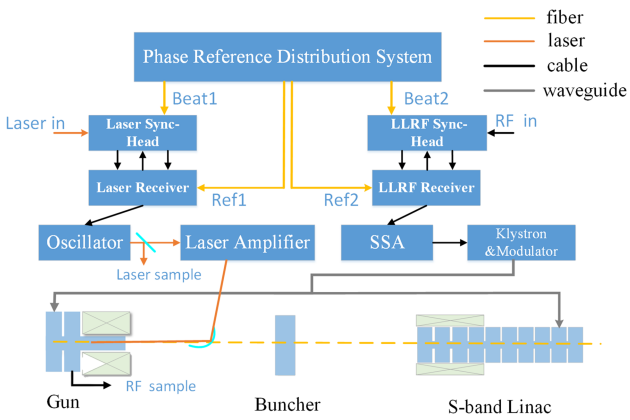

FIG. 6. The deployed timing and synchronization system at the TTX.

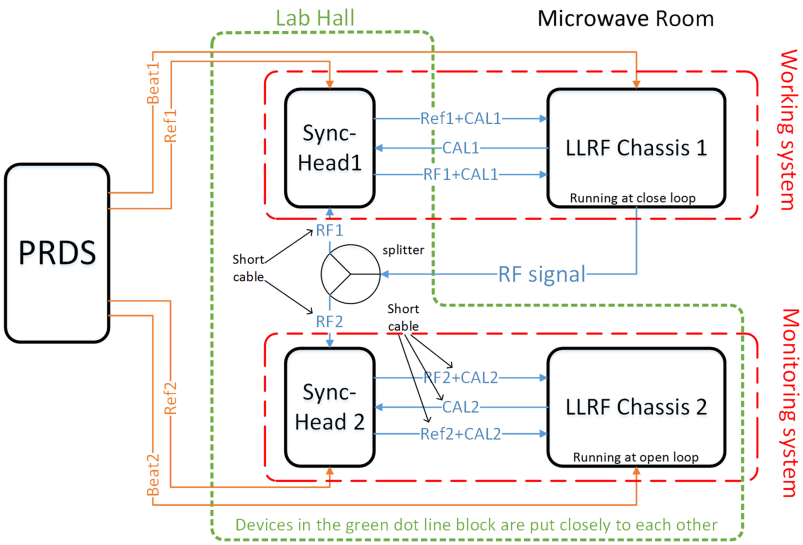

FIG. 7. Mutual monitoring and detecting of two LLRF subsystems.

After the deployment of the whole system, since the PRDS is combined with the laser-RF synchronization or LLRF clients, we evaluate the PRDS with Laser-RF synchronization or LLRF system together instead of measuring the PRDS alone. The test configuration is presented in Fig. 7. Besides, the LLRF chassis 1 and sync-head chassis 1 are the working system which had been deployed in the TTX and run at the closed loop mode; the LLRF chassis 2 and sync-head chassis 2, which are connected with short cables and been set near the sync-head chassis 1, is the monitoring system to estimate the performance of the working system. The reference signals of the two LLRF systems are from the same PRDS. The phase error results detected by the two LLRF systems can be mutually confirmed. Moreover, the two systems' mutual monitoring and detecting experiments will be a convenient and efficient method to evaluate the deployed LLRF system.

In general, the experiment result shows that the LLRF subsystems can effetely reduce the phase jitter in closed loop mode for a long term. The 24-h test result is shown in Fig. 8(a), and the phase error of the working system run at the closed loop mode and the phase error measured by itself is 45.5 fs RMS under 10 Hz sampling speed. By taking the arithmetic mean of subsequences of 100 terms, the moving average (MA) is used to smooth out the drift of the phase error by filtering

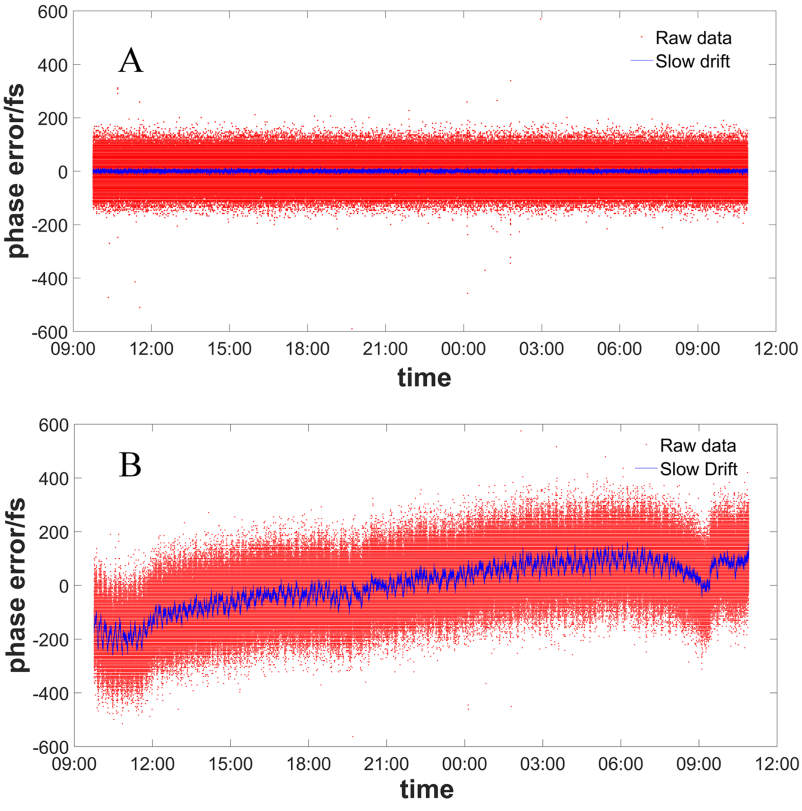

FIG. 8. The test result of the 24-h mutual monitoring and detecting experiment (~8 Hz sampling speed). (a) The working system is running at closed loop mode. (b) The monitoring system is running at open loop and detecting the phase error between the reference and driver RF from the working system.

out the jitter "noise" from random phase error fluctuations. According to the blue line, the drift of the detecting LLRF system is 4.5 fs RMS, which is suppressed to a very low level. After the removal of the slow drift, the jitter noise is 45.3 fs RMS which is the width of the red line and represents the system hardware noise that cannot be reduced by the closed loop correction algorithm.

According to Fig. 8(b), the phase error between the reference and the RF signals generated by the working system is 112 fs RMS, which is detected by the monitoring system. Since LLRF system 2 is run at open loop as a monitor, its phase drift error (the blue line) involves both of the two LLRF systems. The slow drift error is 84.3 fs RMS, which represents the long-term drift between the two LLRF systems. It is mainly caused by the environment temperature drift on the LLRF system chassis and the uncontrolled short cable after the splitter, which has also been observed and proved by lots of daily tests and maintenances. Once the system runs at the closed loop mode, such a drift can be repressed. Therefore, the slow drift can be removed when evaluating the LLRF system performance. The LLRF system phase jitter is 73.5 fs RMS after the removal of the slow drift. Since the phase error of the monitoring system is the sum of the two independent systems, the real phase jitter of one LLRF system should be $73.5/\sqrt{2} = 52.0$ fs RMS, which is almost equal to that of the working LLRF system (45.3 fs). Besides, both systems' test results can be a mutual validation that the phase jitter of the LLRF system is near 50 fs RMS.

In addition, the mutual monitoring and detecting experiments can also be applied to the laser-RF synchronization system. However, the receiver chassis and sync-head chassis is quite near, and both of them have been put in the room with constant temperature and humidity with the PRDS, the temperature drift is limited, and the signal source analyzer can adequately take the system performance assessment because it is a CW signal, and the Laser-RF synchronization test will be shown in Sec. IV B.

B. The test results of the PRDS combined with laser-RF synchronization and LLRF system

The mutual monitoring and detecting experiments are suitable for the system self-test after the system chassis manufacturing. After the deployment, the online tests of the subsystems of timing and synchronization system along with the other system on the accelerator (high power system, laser oscillator, etc.) are also needed.

Before the laser-RF synchronization system is deployed at the real oscillator, a laser oscillator emulator has been made for control loop evaluation. The final laser oscillator close phase noise is 48.2 fs RMS (10 Hz–100 kHz) with the emulator, which represents the ideal working situation of the system. The laser oscillator emulator test proved that the phase locking algorithm of laser-RF synchronization can work properly.[25] After the system deployment on the mode-locked Ti:sapphire oscillator (central wavelength at 800 nm, manufactured by Coherent, Inc.), the working performance on the real laser oscillator is measured with the E5052B signal source analyzer. We measured the harmonic frequency (2856 MHz) signal that is coupled from the photodiode in the sync-head chassis. The absolute integral phase noise of the signal is among 80–100 fs RMS, and the typical result is shown in Fig. 9, whose jitter is 83.2 fs RMS (10 Hz–100 kHz) in the closed-loop mode. Under the open-loop mode, the laser oscillator could integrate several picoseconds of phase noise RMS.

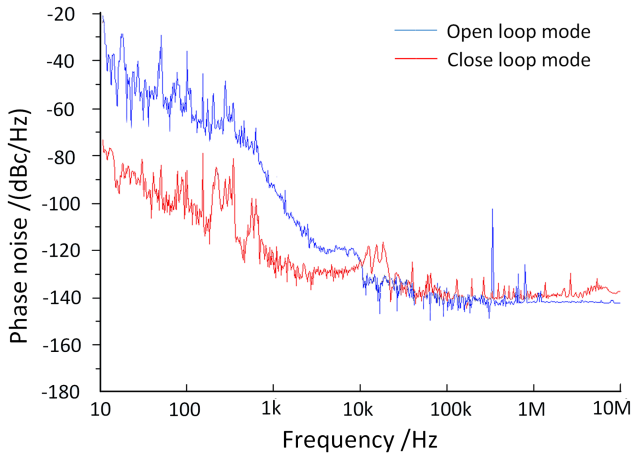

FIG. 9. Laser-RF synchronization result measured by Agilent E5052B signal source analyzer.

As shown in Fig. 9, the phase noise of the low frequency parts has been suppressed significantly. For the feedback loop bandwidth in tens kHz, we cannot detect and deal with the high-frequency noise (higher than 100 kHz) of the oscillator. The most part of measured noise above 100 kHz might come from the shot noise of the photodiode, the thermal noise of the RC electronic components, and the flicker noise of MOSFETs. Regarding the approximately −140 dBc/Hz line in Fig. 9, the shot noise can be lowered by increasing the light power shooting the photodiode. Although the AM-PM conversion influence has been reduced evidently in our digital phase detector scheme system,[25] the AM-PM effect in the E5052B signal source analyzer may also make a contribution to the measured phase noise above 100 kHz during detection. In addition, the oscillator should be preheating to be working stabilized after system boot to reduce its high-frequency noises in order to achieve high-precision phase-locked. According to the closed loop mode line in Fig. 9, there is a crest near 10 kHz-20 kHz in the noise spectrum of the closed loop laser oscillator, which is limited by the bandwidth of the PZT and the high-voltage amplifier, and the circuit will also be improved in the subsequent revision.

After the LLRF system deployment on the TTX, the same set of the LLRF system was used to measure the phase jitter of the deployed LLRF system with the related high-power system (the solid-state amplifier and the high voltage modulator) by comparing the signals from different pickup points of the system with the reference signal from the same PRDS. Suppose the LLRF system and the high-power system are independent of each other, we can obtain the impact of noise of each section by a separate test. We can yield 46 fs RMS phase jitter under closed loop of the LLRF sync-head and receiver chassis self-test by careful circuit optimization. By using the same measurement method, the phase jitter test

result of the LLRF sync-head and receiver chassis plus SSA is 126 fs RMS. Therefore, the impact of the SSA can be calculated by $\sqrt{126^2 - 46^2} = 118$ fs RMS. The online test of the whole system result shows that the signal RMS jitter is about 225 fs. Similarly, it can be calculated that the noise from the high-voltage modulator and klystron is $\sqrt{225^2 - 118^2} = 190$ fs RMS. To achieve better performance of the LLRF system, the solid-state amplifier and high-voltage modulator are considered to upgrade in the future.

C. Beam-based phase jitter measurement experiment

The tests in Secs. IV A and IV B are the system self-assessment to characterize the timing and synchronization system performance. Besides, a beam-based method[29] is also applied to measure the jitter between the photocathode driving laser and the RF phase in the photocathode RF gun, which are close loop controlled by the laser synchronization client and LLRF client, respectively. These measurements help us to evaluate the performance of the synchronization system and find the possible jitter source in the whole facility.

The typical experimental result is shown in Fig. 10. The experiment's duration is about 80 min. The measured RF-to-laser phase error in the photocathode RF gun is about 728 fs RMS, which includes a slow-drift phase error, shown by the blue line [Fig. 10(a)]. The fast Fourier transformation of the total phase error jitter is shown in Fig. 11(a) to indicate the phase errors each time scale contributes. The peak frequency is $f_1 = 2.29 \times 10^{-4}$ Hz. It illustrates that the phase error of the total phase error jitter mostly comes from the slow drift. After subtracting the slow drift, the remaining phase jitter is 277 fs RMS [Fig. 10(b)].

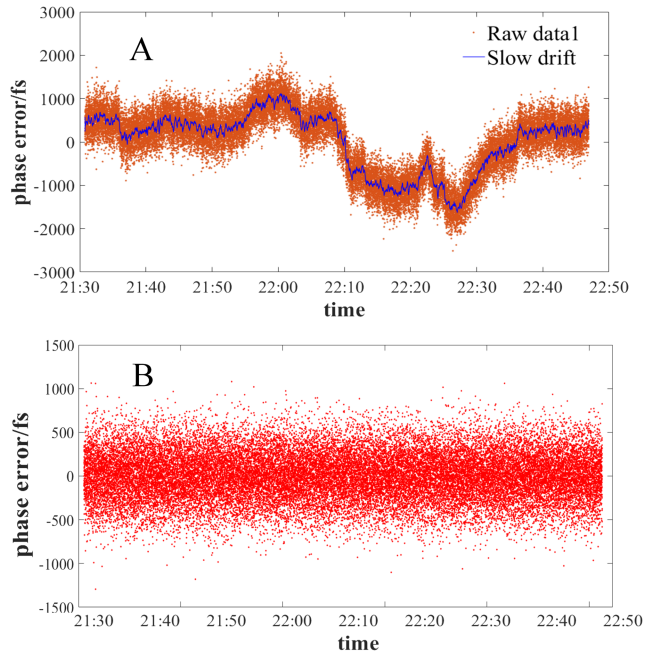

FIG. 10. The phase error jitter between microwave and laser in the experiments (~8 Hz sampling speed). (a) The total phase error and slow drift, and the slow drift is shown in the solid blue line. (b) The phase jitter after removing the slow drift is 277 fs RMS, which indicates the optimal performance status of the timing and synchronization system.

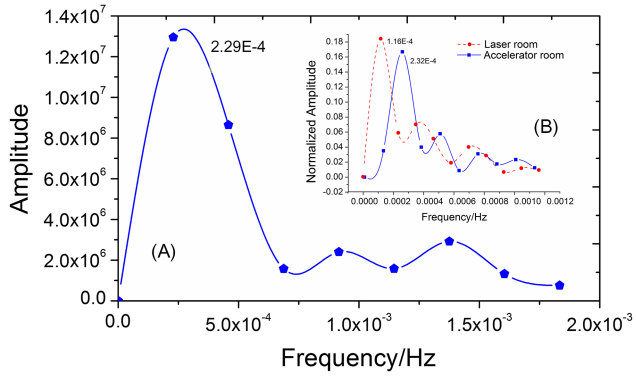

FIG. 11. The fast Fourier transformation of the phase error jitter and the environment temperature in the experiments. (a) The Fourier transform of the total phase error, and the peak frequency is $f_1 = 0.229$ mHz. (b) The Fourier transform of the accelerator hall and the laser room temperature, and the frequencies of the two peaks are $f_2 = 0.232$ mHz and $f_3 = 0.116$ mHz, respectively; f_3 is less than f_2 for the temperature stability requirement in the laser room are much stricter than that in the accelerator room.

The large slow drift effect may be attributed to the temperature change of the lab environment (~1 °C peak to peak) that includes the accelerator hall and the laser clean room. The RF source pickup point and the LLRF sync-head chassis is connected by a ~10 cm RG316 RF coaxial cable (as a port adapter) and a ~100 cm FSJ2 phase stabilized cable, which is out of the control loop. Hence, the temperature variation of the cables will directly lead to phase error drift. The Fourier transformation of the total phase error and the environment temperature are presented in Fig. 11(b). The peak temperature frequency of the experiment hall ($f_2 = 0.232$ mHz) is quite near the phase error jitter peak frequency ($f_1 = 0.229$ mHz), which indicates that the phase error slow drift mainly results from the temperature variation in the accelerator room. The cycle time of the hall temperature is ~72 min, being consistent with the phase error drifts (~73 min). For a common solid Polytetrafluoroethylene (PTFE) dielectric cable, the temperature coefficient is over 150 ppm/°C (25–35 °C), and the temperature coefficient of the FSJ2 phase stabilized cable is about 10 ppm/°C (20–40 °C). Therefore, the phase change of the two cables caused by 1 °C is about 200 fs, making a contribution to the slow drift (±1000 fs scale) in Fig. 10.

Another phase error drift source comes from the laser amplifier and the follow-up long optical path and its transmission, which are also out of the control loop in the laser-RF synchronization system. Although the mode-locked laser oscillator is in the high-precision phase locked mode, the temperature change will lead to a certain degree of phase shift at last. According to Fig. 11(b), the peak frequency of the laser clean room temperature ($f_3 = 0.116$ mHz) is also close to the peak frequency of the slow phase error drift that will affect the experimental result. However, it is difficult to estimate the exact effect with the current method since the laser power is too high. Moreover, the laser sample fiber (~1 m) between the pickup point and the laser sync-head chassis is also out of the control loop of the system. The typical fiber temperature coefficient is 5 ppm/°C, so the phase change of

the pickup fiber caused by 0.5 °C is about 10 fs, which can be ignored due to its little impact on the whole system phase jitter.

In general, the slow drift mainly origins from the effect of temperature drift on the out of control loop parts in the TTX timing and synchronization system. The drift can be suppressed and eliminated with an appropriate slow feedback loop added for the actual accurate feedback needs. We have used the electro-optic (EO) based technique to implement as a beam arrival time detection and timing jitter recoding to do the feedback to get rid of the phase error drift, and it will be reported in another journal paper soon. Besides, the cable between the RF pickup points will also be replaced with a shorter phase stabilized cable to reduce its effect on the slow drift caused by temperature variation. Therefore, after the removal of the slow drift for the current system evaluation, the phase jitter is 277 fs RMS, mostly representing the optimal overall system performance.

During the beam-based experiment, the phase jitter of the subsystems is also simultaneously measured, and the LLRF control loop phase jitter after the klystron is 245 fs RMS including the ~50 fs RMS LLRF system chassis jitter, ~230 fs RMS SSA, and modulator's jitter. The laser-RF synchronization measured 106 fs RMS (10 Hz–100 kHz) by using the signal source analyzer. The different noises are considered to be independent. Therefore, the total noise contribution of the two synchronized clients is $\sqrt{245^2 + 106^2} = 267$ fs, which is consistent with the phase jitter (277 fs RMS) in the experiment.

V. SUMMARY AND DISCUSSION

The integrated high-precision timing and synchronization system is realized in the Tsinghua University, and the CW laser based PRDS has achieved a good accuracy of reference distribution. Besides, two typical client's systems, the LLRF system and the laser-RF synchronization system, are also built and work properly for the phase control of the RF and laser. An asymmetric calibration sideband CAL signal method is proposed to eliminate the non-linear distortion during the long cable signal transmission. The phase jitter under closed loop of the LLRF system with the PRDS is nearly 46 fs RMS for 24-h test. The digital phase detector is applied to make the phase measurement in the laser-RF synchronization and both fundamental and harmonic signals are used to achieve the high precision of the system. In addition, the absolute integral phase jitter of laser-RF synchronization system with the PRDS is typically 83.2 fs RMS (10 Hz–100 kHz) by the Agilent E5052B signal source analyzer.

After the system deployment in the TTX, the main sources of the phase error noise of the subsystems are measured carefully and analyzed clearly, which will be conductive to the future system upgrade. Regarding the LLRF system, a majority percent of jitter comes from the noise of the high-voltage modulator, which needs to be upgraded later for the system better performance. A LLRF subsystem's mutual monitoring and detecting test is proposed and applied on the deployed LLRF system, which is proved to be a convenient and efficient way to evaluate the LLRF subsystem. The beam-based experiment based on a high time resolution method evaluates the whole timing and synchronization system in another view, showing the total system phase jitter is 277 fs RMS after subtracting the slow drift. Meanwhile, 277 fs RMS phase jitter matches with the sum of the subsystems' phase jitter 267 fs RMS measured. The experiment provides a performance evaluation method for the high-precision timing and synchronization system. The scheme of the timing and synchronization system in the THU can be expanded to synchronize tightly dozens of RF and optical sources for future requirements on the km-scale facilities.

In the future system design, a feed forward module is under construction to treat the predictable distortion such as the slow drift. It will include the beam arrival time detection device (BAM) and the modulator high-voltage feed forward submodule. By adjusting the phase parameters of other control clients, the feed forward module can compensate the influence of predictable phase error sources, such as the klystron high voltage jitter and the temperature drift effect on the out-of-loop parts of the system.

ACKNOWLEDGMENTS

This work was supported by the National Natural Science Foundation of China (NSFC Grant Nos. 11375097 and 11475097). The author is especially grateful to Dan Zhang, Zhichao Sun, and all the other colleagues from HZCY company for their help in chassis manufacturing, debugging, and the assistance in the experiment.

[1] R. Li, C. Tang, Y. Du, W. Huang, Q. Du, J. Shi, L. Yan, and X. Wang, Rev. Sci. Instrum. **80**, 083303 (2009).
[2] R. Li, W. Huang, Y. Du, L. Yan, and Q. Du, Rev. Sci. Instrum. **81**, 36110 (2010).
[3] P. Musumeci, J. T. Moody, and C. M. Scoby, Ultramicroscopy **108**, 1450 (2008).
[4] J. B. Hastings, F. M. Rudakov, D. H. Dowell, J. F. Schmerge, J. D. Cardoza, J. M. Castro, S. M. Gierman, H. Loos, and P. M. Weber, Appl. Phys. Lett. **89**, 184109 (2006).
[5] L. H. Yu, L. DiMauro, A. Doyuran, W. S. Graves, E. D. Johnson, R. Heese, S. Krinsky, H. Loos, J. B. Murphy, G. Rakowsky, J. Rose, T. Shaftan, B. Sheehy, J. Skaritka, X. J. Wang, and Z. Wu, Phys. Rev. Lett. **91**, 074801 (2003).
[6] L. H. Yu and I. Ben-Zvi, Nucl. Instrum. Methods Phys. Res., Sect. A **393**, 96 (1997).
[7] I. Ben-Zvi, L. F. Di Mauro, S. Krinsky, M. G. White, and L. H. Yu, Nucl. Instrum. Methods Phys. Res., Sect. A **304**, 181 (1991).
[8] A. Ting, R. Fischer, A. Fisher, C. I. Moore, B. Hafizi, R. Elton, K. Krushelnick, R. Burris, S. Jackel, K. Evans, J. N. Weaver, P. Sprangle, E. Esarey, M. Baine, and S. Ride, Nucl. Instrum. Methods Phys. Res., Sect. A **375**, ABS68 (1996).
[9] R. W. Schoenlein, W. P. Leemans, A. H. Chin, and P. Volfbeyn, Science **274**, 236 (1996).
[10] Y. Du, L. Yan, J. Hua, Q. Du, Z. Zhang, R. Li, H. Qian, W. Huang, H. Chen, and C. Tang, Rev. Sci. Instrum. **84**, 053301 (2013).
[11] C. Tang, W. Huang, R. Li, Y. Du, L. Yan, J. Shi, Q. Du, P. Yu, H. Chen, T. Du, C. Chen, and Y. Lin, Nucl. Instrum. Methods Phys. Res., Sect. A **608**, S70 (2009).
[12] K. Czuba, K. Antoszkiewicz, S. Simrock, and H. Weddig, in *Proceedings of PAC09, Vancouver, BC, Canada* (JACoW, 2009), p. 2255.
[13] R. Zeng and A. J. Johansson, in *Proceedings of IPAC2013, Shanghai, China* (JACoW, 2013), p. 3379.
[14] J. Kim, J. A. Cox, J. Chen, and F. X. Kärtner, Nat. Photonics **2**, 733 (2008).
[15] M. Y. Peng, "Sub-femtosecond optical timing distribution for next-generation light sources," Ph.D. thesis, Institute of Technology, Massachusetts, 2015, https://dspace.mit.edu/handle/1721.1/101467.

[16]R. Wilcox, J. M. Byrd, L. Doolittle, G. Huang, and J. W. Staples, Opt. Lett. **34**, 3050 (2009).
[17]G. Huang, L. R. Doolittle, J. W. Staples, R. Wilcox, and J. M. Byrd, in *Proceedings of BIW10, Santa Fe, New Mexico, USA* (JACoW, 2010), p. 375.
[18]F. X. Kartner, F. O. Ilday, J. Kim, A. Winter, F. Grawert, H. Byun, and J. Chen, in *Proceedings of PAC 2005* (IEEE, Knoxville, Tennessee, 2005), p. 284.
[19]S. Michizono, H. Katagiri, T. Matsumoto, T. Miura, Y. Yano, and S. Fukuda, in *Proceedings of LINAC08, Victoria, BC, Canada* (JACoW, 2008), p. 1048.
[20]M. E. Angoletta, J. Bento, A. Blas, E. Bracke, A. Butterworth, F. Dubouchet, A. Findlay, F. Pedersen, and J. Sanchez-Quesada, in *Proceedings of IPAC2010, Kyoto, Japan* (JACoW, 2010), p. TUPEA057.
[21]M. Ferianis, A. Borga, A. Bucconi, L. Pavlovic, M. Predonzani, and F. Rossi, in *Proceedings of FEL2011, Shanghai, China* (JACoW, 2011), p. 641.
[22]M. Xin, K. Safak, M. Y. Peng, A. Kalaydzhyan, W. Wang, O. D. Mücke, and F. Kaertner, Light: Sci. Appl. **6**, e16187 (2017).
[23]J. D. Deschênes, L. C. Sinclair, F. R. Giorgetta, W. C. Swann, E. Baumann, H. Bergeron, M. Cermak, I. Coddington, and N. R. Newbury, Phys. Rev. X **6**, 021016 (2016).
[24]J. Yang, W. Huang, Y. Xu, D. Wang, Y. Du, and Y. Yan, in *Proceedings of IPAC2016, Busan, Korea* (JACoW, 2016), p. 4237.
[25]J. Yang, Y. Du, L. Yan, G. Huang, Q. Du, Y. Xu, W. Huang, and H. Chen, Nucl. Sci. Tech. **28**(4), 57 (2017).
[26]Z. Lin, J. Yang, Y. Du, Y. Xu, W. Huang, C. Tang, G. Huang, Q. Du, L. Doolittle, R. Wilcox, and J. Byrd, in *Proceedings of IPAC2017, Copenhagen, Denmark* (JACoW, 2017), p. 4565.
[27]Q. Du, Y. Du, L. Yan, W. Huang, J. Li, and C. Tang, Nucl. Instrum. Methods Phys. Res., Sect. A **637**, S137 (2011).
[28]L. Doolittle, H. Ma, and M. S. Champion, in *Proceedings of LINAC2006, Knoxville, Tennessee, USA* (JACoW, 2006), p. 568.
[29]Z. Zhang, Y. Du, L. Yan, Q. Du, J. Hua, J. Shi, J. Yang, D. Wang, W. Huang, H. Chen, and C. Tang, Phys. Rev. Spec. Top.–Accel. Beams **17**, 032803 (2014).